MEDICAL RADIOLOGY
Diagnostic Imaging

Editors:
A. L. Baert, Leuven
K. Sartor, Heidelberg

R. Maroldi · P. Nicolai (Eds.)

Imaging in Treatment Planning for Sinonasal Diseases

With Contributions by

A. R. Antonelli · G. Battaglia · M. Berlucchi · A. Bolzoni · A. Borghesi · D. Farina
D. Lombardi · P. Maculotti · R. Maroldi · I. Moraschi · P. Mortini · F. Mossi · P. Nicolai
L. Palvarini · L. Pianta · C. Piazza · L. Pinelli · V. Portugalli · L.O. Redaelli de Zinis
D. Tomenzoli

Series Editor's Foreword by

A. L. Baert

Foreword by

W. Draf

With 268 Figures in 620 Separate Illustrations, 44 in Color and 14 Tables

Springer

Roberto Maroldi, MD
Professor, Department of Radiology

Piero Nicolai, MD
Professor, Department of Otorhinolaryngology

University of Brescia
Piazzale Spedali Civili 1
25123 Brescia, BS
Italy

Medical Radiology · Diagnostic Imaging and Radiation Oncology
Series Editors: A. L. Baert · L. W. Brady · H.-P. Heilmann · M. Molls · K. Sartor

Continuation of Handbuch der medizinischen Radiologie
Encyclopedia of Medical Radiology

ISBN 3-540-42383-4 Springer Berlin Heidelberg New York

Library of Congress Cataloging-in-Publication Data

Imaging in treatment planning for sinonasal diseases / R. Maroldi, P. Nicolai (eds.) ; with contributions by A. R. Antonelli ... [et al.] ; foreword by A. L. Baert.
p. ; cm. -- (Medical radiology)
Includes bibliographical references and index.
ISBN 3-540-42383-4 (alk. paper)
1. Paranasal sinuses--Imaging. 2. Nose--Imaging. 3. Paranasal sinuses--Diseases--Diagnosis. 4. Nose--Diseases--Diagnosis. 5. Paranasal sinuses--Diseases--Treatment. 6. Nose--Diseases--Treatment. I. Maroldi, R. (Roberto), 1954- II. Nicolai, P. (Piero), 1954- III. Antonelli, A. R. IV. Series.
[DNLM: 1. Paranasal Sinus Diseases--diagnosis. 2. Paranasal Sinus Diseases--therapy. 3. Diagnostic Imaging--methods. WV 340 I31 2004]
C8255 2004]
RF345.I446 2004
616.2'107'54--dc22 2004045232

Springer is part of Springer Science+Business Media

http//www.springeronline.com

Printed in Germany

Medical Editor: Dr. Ute Heilmann, Heidelberg
Desk Editor: Ursula N. Davis, Heidelberg
Production Editor: Kurt Teichmann, Mauer
Cover-Design and Typesetting: Verlagsservice Teichmann, 69256 Mauer

Printed on acid-free paper – 21/3150xq – 5 4 3 2 1 0

To *Elisabetta* and *Daniela*,
for their support and patience

Roberto and Piero

Series Editor's Foreword

This volume not only provides a modern multimodality imaging approach to the pathology of the sinonasal area, based on CT, MR imaging and endoscopy, but also focuses on the treatment strategy and the role of imaging in the decision-making process for each individual patient.

The combined interdisciplinary approach by a radiologist and an ENT surgeon gives this book unique clinical value.

The different chapters comprehensively cover imaging modalities, anatomy, physiology and the complete spectrum of sinonasal diseases. The volume as a whole is eminently readable and superbly illustrated.

The content represents mainly the approach of the editors' institution, based on long clinical experience and innovative research, but also covers other modern views and concepts.

This outstanding volume will serve the needs not only of general radiologists dealing daily with the common sinonasal conditions but also of specialised head and neck radiologists. It can also be recommended highly as an invaluable reference not only to radiologists but also to ENT specialists.

I am confident that this excellent book will meet the same success as previous volumes published in this series.

Leuven — Albert L. Baert

Foreword

The time should have passed when the radiologist produced the images he was asked for and the ENT surgeon took them and made his own interpretation as the basis for the decision on conservative or surgical treatment.

The optimal information from images is obtained from interdisciplinary discussion, sitting together as long as time allows. Without a doubt the neuroradiologist or the head and neck radiologist can describe the imaging findings in the most detailed way. On the other hand he or she depends to a high degree on the hopefully precisely formulated questions of the clinical partner. Sometimes the interdisciplinary discussion results in the recommendation of further imaging by the radiologist. This personal contact with the specialty clinician also ensures familiarity with the latest therapeutic options, which eases the interpretation of postoperative images.

This monograph combines in an ideal way the expertise of a superbly skilled head and neck radiologist and a rhinologist who is one of the pioneers of modern endonasal surgery, using endoscope and microscope as indispensable surgical tools. The book gives clear guidance on the necessary imaging and the findings, as well as interpretation of all types of nose and sinus pathology and general guidelines for treatment, particularly surgery, resulting from interdisciplinary discussion. It deals with anatomy, CT and MR techniques of study, inflammatory diseases, tumors, and post-treatment imaging. This is a particularly effective way forward in one of the most fascinating fields of modern otorhinolaryngology.

I wish this book a wide readership among neuroradiologists and head and neck radiologists, as well as ENT, head and neck, and maxillo-facial surgeons.

Fulda — Wolfgang Draf

Preface

As there are already many books on imaging of sinonasal tract diseases, one might wonder, "Why bother to compile another one?". In responding to this question, it must be emphasized that cross-sectional imaging (i.e., computed tomography and magnetic resonance) has clearly been one of the backbones which has made possible, in the last decade, the remarkable evolution of treatment strategies for sinonasal tract diseases, in particular microendoscopic sinus surgery.

The purpose of this volume is to provide the knowledge required to properly solve the challenging issues raised by current treatment planning. Accordingly, this book is intended not only for the head and neck expert, or the general radiologist, but for the entire team of physicians (otorhinolaryngologist, maxillo-facial surgeon, radiotherapist, and oncologist) that participate in the decision-making process and who need to be confident with the indications, limitations, and advantages of state-of-the-art imaging techniques.

The book is organized into three main sections. In the first, general aspects such as CT and MR techniques, as well as anatomy and physiology, are thoroughly discussed. In addition, we decided to include a detailed guide to imaging assessment of critical issues, such as bone, orbit, and skull base invasion, in this section. The section is completed by an indispensable overview of a wide spectrum of surgical approaches for the sinonasal tract.

The second part of the book provides step-by-step information on the basic and advanced aspects of clinical presentation, imaging findings, and treatment of sinonasal diseases. For each specific disease, the rationale underlying the treatment strategy is discussed and the imaging findings critical to the decision-making process are identified and discussed. This approach reflects the constant team effort of our two departments, radiology and otorhinolaryngology, over the past 15 years towards integration of clinical and radiological information with the aim of establishing the most appropriate treatment. Special emphasis is placed on the identification of clinical and imaging data that allow selection of a microendoscopic or an external approach in candidates for surgery.

In the third part, the challenging issue of imaging acute or late complications and recurrent lesions is discussed in detail. Moreover, the integration of endoscopic and radiological follow-up in different diseases is thoroughly reviewed. As the book reflects the radiological and clinical experience of a single institution, two topics, namely traumatic lesions and congenital malformations, were not covered as we do not have the required expertise in these fields. We believe that through the correlation of imaging with endoscopic or clinical findings, this book will enable radiologists to familiarize themselves with a more "otorhinolaryngological" point of view and will help clinicians

to understand more fully the significance of specific radiological findings. It will also serve as a guide for the selection of imaging techniques.

Finally, we would like to acknowledge Prof. Chiesa (Head of the Department of Radiology) and Prof. Antonelli (Head of the Department of Otorhinolaryngology) who promoted the active cooperation between these two specialties at our university. Without their invaluable support, as well as that of younger colleagues, the writing of this book would have been an impossible challenge.

Brescia

Roberto Maroldi
Piero Nicolai

Contents

1 Techniques of Radiological Examination

Davide Farina and Andrea Borghesi

CONTENTS

1.1 Incremental and Single-Slice Spiral CT Technique

1.1.1 CT Protocol Chronic Rhinosinusitis and Nasal Polyposis

1.1.1.1 Patient Preparation

Patients affected by chronic rhinosinusitis must receive adequate medical treatment before CT examination of the paranasal sinuses, in order to treat acute infection and solve mucosal edema. Oral antibiotics, nasal steroids and antihistamines – prescribed at least 3 weeks before CT – decrease the risk of overestimating chronic inflammation and polypoid reaction of the mucosa. Additionally, according to the recommendations of several authors, patients should be asked to clear their nose before undergoing the examination (Oliverio et al. 1995; Phillips 1997; Zinreich 1998).

D. Farina, MD; A. Borghesi, MD
Department of Radiology, University of Brescia, Piazzale Spedali Civili 1, Brescia, BS, 25123, Italy

Radiation dose is a major concern, especially when CT examination is performed as a screening or presurgical test, in a population that includes a large number of young subjects. In this setting, the rationale of imaging studies is to obtain detailed information on patency/occlusion of mucous drainage pathways, on bone changes (particularly in critical areas such as the skull base and orbit), intrasinusal content (air, fluid, solid, calcifications), and on anatomic variants. As a consequence, conventional radiology should be discarded as an obsolete tool, even though the overall radiation dose delivered to the eye-lens with this technique is rather low (approximately 0.57 mGy) (Zammit-Maempel 1996; Phillips 1997; Zinreich 1998; Sievers et al. 2000).

Computed tomography is a relatively high-dose examination, nevertheless the high natural contrast between air, mucosa and bone enables optimization of low-dose protocols by decreasing tube current down to 30–50 mAs (MacLennan 1995; Hein et al. 2002; Hagtvedt et al. 2003). This results in a considerable decrease of the eye-lens dose (3.1 mGy when 50 mAs are applied) (Sohaib et al. 2001) without significant loss of diagnostic information. With MSCT scanners, patient exposure is a primary issue. Recent data demonstrate eye-lens dose higher than single-slice (SS) scanners, even when low-dose protocols (40 mAs) are applied (9.2 mGy). Nevertheless, also with this new tool, exposure is far below the threshold for detectable lens opacities (0.5–2 Gy) (Zammit-Maempel et al. 2003).

1.1.1.2 Direct Coronal Plane Acquisition

Images are electively acquired on coronal plane, as perpendicular to the hard palate as permitted by gantry tilting and patient cooperation. This plane is able to demonstrate patency, width, and morphology of all those airspaces (middle and superior meatus, ethmoid infundibulum) hidden by turbinates and therefore difficult to access at clinical examination. Moreover, coronal imaging clearly depicts both superior and lateral insertion of the middle turbinate, and the cribriform

plate. The main weaknesses of this scanning orientation are the poor delineation of the frontal recess (coursing along an oblique-sagittal plane), as well as the impossibility to demonstrate sinusal walls lying in the coronal plane.

Two options are described for patient positioning: supine, with hyperextended head (hanging-head position) (Phillips 1997), or prone. The latter is usually preferred because it is more easily tolerated by the patient and less susceptible to motion artifacts. Additionally, fluid material retained in a maxillary sinus, in the hanging-head position will freely flow towards the ostium, therefore impairing the evaluation of its patency.

The examination area extends from the anterior frontal sinus wall to the posterior border of the sphenoid sinus. Scanning parameters are highly variable according to the clinical issues to be addressed and to the available equipment (Zinreich 1998). In our experience, optimal demonstration of the ostiomeatal unit and of natural drainage pathways is achieved with:

- Thin slice collimation (1–2 mm), to minimize partial volume artifacts that may mimic mucosal thickenings along small caliber drainage pathways.
- 3- to 4-mm increment/1.5 pitch (sequential or SS spiral equipment, respectively) as a trade-off between dose reduction and the necessity not to miss anatomical structures such as the uncinate process (Table 1.1).

For sinus screening purposes, sufficient information can be obtained with thicker collimation (3–5 mm) and an increment of up to 15 mm.

Table 1.1. Chronic rhinosinusitis, nasal polyposis: scanning parameters, coronal plane

Parameters	Sequential CT	SSCT
Slice thickness	1 mm	2 mm
Increment/ pitch	3 mm	Pitch 1,5
mA/kV	70/133	60/120÷140
Reconstruction algorithm – *kernel**	*Ultrahigh*	A 70÷90

SSCT, single-slice spiral technique. * Siemens equipment

1.1.1.3 Axial Plane Acquisition

This scanning plane enables adequate demonstration of some anatomical structures difficult to assess on coronal plane due to their spatial orientation (such as posterior frontal sinus and sphenoid sinus wall, sphenoethmoid recess). Nonetheless, axial acquisition is recommended only whenever the digital lateral view (topogram) shows excessive dental amalgam or metallic implants, or as a complement after coronal scanning whenever precise information on specific anatomic structures is required.

In the first condition, a data set of thin and contiguous (to avoid aliasing) slices may be acquired with the incremental technique (1–2 mm collimation) or the SS spiral technique (2 mm collimation; pitch 1–1.5; 1–2 mm reconstruction) (Table 1.2). The patient lies in supine position, both his/her sagittal plane and hard palate should be perpendicular to the gantry's scan line, in order to achieve, respectively, optimal symmetry of the anatomical structures on axial plane, and no/minimal gantry tilting. In fact, the quality of MPR is degraded by gantry inclination (stair-step artifacts). Direct scans should be oriented parallel to the hard palate and range from the upper border of frontal sinuses to the alveolar process of maxillary bones; nasal tip and petrous bone should be included in the field of view. Subsequent coronal MPR reformation is obtained for proper assessment of critical anatomical areas either at risk of iatrogenic damage (cribriform plate, fovea ethmoidalis) or playing a key role in mucous drainage (ostiomeatal unit).

When acquired as a complement to the coronal study, axial scans are basically focused on anatomical areas inadequately demonstrated in that orientation (i.e., anterior and posterior walls of maxillary, frontal, and sphenoid sinus, sphenoethmoid recess). Additionally, this scan plane is valuable for the detection of Onodi cells. In this setting, contiguous slices and full coverage of the paranasal area are generally unnecessary, as a consequence, 4- to 5-mm increments can be applied, decreasing both patient exposure and examination time.

Table 1.2. Chronic rhinosinusitis, nasal polyposis: scanning parameters, axial plane

Parameters	Sequential CT	SSCT
Collimation	1÷2 mm	2 mm
Increment/ pitch	1÷5 mm	Pitch 1÷1,5
mA/kV	70/133	60/120÷140
Reconstruction algorithm – *kernel**	*Ultrahigh*	A 70÷90
MPR	COR/SAG	Idem

SSCT, single-slice spiral technique; MPR, multiplanar reconstruction; COR, coronal; SAG, sagittal. * Siemens equipment

1.1.2 CT Protocol in Neoplastic Lesions

The first step in the diagnostic work-up of both benign and malignant sinus neoplasms consists of fiberoptic examination. Endoscopy allows adequate demonstration of the superficial spread of the lesion and may guide a biopsy. The discrimination between benign and malignant tumors and the precise characterization of the lesion are, in most cases, far beyond the capabilities of CT. The main goals of imaging are, therefore, to provide a precise map of deep tumor extension in all those areas blinded at fiberoptic examination, especially anterior cranial fossa, orbit, and pterygopalatine fossa.

In this setting, MR is the technique of choice for several reasons:

- It clearly differentiates tumor from retained secretions
- It allows early detection of perivascular/perineural spread
- It allows higher contrast resolution

On the other hand, the strengths of CT consist of:

- Superior definition of bone structures even in the case of subtle erosions
- Faster and easier performance
- Superior accessibility and lower cost.

As a consequence, in our experience CT indications are restricted to patients who have not undergone a preliminary examination by the otolaryngologist (to rule out non-neoplastic lesions) or to patients bearing contraindications to MR.

1.1.2.1 Axial Scanning

CT protocol consists of native and post-contrast scanning in both axial and coronal planes; it is preferable to start the examination on the axial plane and to complete it with coronal scans, usually limited to the area of the lesion. Both incremental and spiral techniques can be applied, though the latter is faster and requires lower doses of contrast agent.

On the axial plane, the gantry must be parallel to the hard palate. The examination area extends from the superior border of the frontal sinus to the alveolar process of the maxillary bone. Scans are acquired with 2- to 3-mm collimation, 2- to 3-mm increments (sequential CT), pitch 1–1.5 (SS spiral equipment) (Table 1.3). The fastest rotation time should be applied to decrease the risk of motion artifacts. A high contrast resolution is mandatory, therefore a higher radiation dose is required (200–240 mAs, 140 kV) and both soft tissue and bone algorithms are adopted for image reconstruction.

Table 1.3. Neoplasm staging. scanning parameters, axial plane

Parameters	Sequential CT	SSCT
Orientation	Parallel to hard palate	Idem
Collimation	2÷3 mm	2÷3 mm
Increment/ pitch	2÷3 mm	Pitch 1÷1,5
mA/kV	200-240/140	200-240/140
Reconstruction algorithm	*Soft tissue/ bone*	Idem
MPR	COR/SAG	Idem

SSCT single-slice spiral technique; MPR, multiplanar reconstruction; COR, coronal; SAG, sagittal.

Contrast agent protocol consists of biphasic injection (80–90 ml at a rate of 2.5 ml/s plus 30–40 ml at a rate of 1–1.5 ml/s), and a scanning delay of approximately 80 s. This time interval enables an assessment of the lesion in its window of more intense enhancement, therefore maximizing the detection of lesion boundaries (Maroldi et al. 1998). Early acquisition in the arterial phase (30s delay) may be indicated when a highly vascular lesion is suspected or to precisely delineate the relationships between the neoplasm and the carotid arteries.

1.1.2.2 Coronal Scanning

Scanning parameters in the coronal plane are comparable to those used for the axial plane. Additional contrast agent administration (40–50 ml at a rate of 2 ml/s) may be suggested. Whenever prone positioning is impossible to obtain, the patient is scanned exclusively in the axial plane (contiguous 2-mm thick slices, no gantry tilting) and multiplanar reconstructions are subsequently obtained.

1.2 Multislice CT of the Paranasal Sinuses

Improvements in CT imaging of the paranasal sinuses provided by multislice technology include fast coverage of the volume of interest, thin collimation (up to 0.75 mm with 16-row MSCT), and acquisition of

nearly isotropic (i.e., cubic) voxels. The latter results in high quality multiplanar reformation of the data set, preferably acquired on the axial plane. According to the number of detectors of the equipment employed, the volume of interest is acquired from 4×1 mm up to 16×0.75 mm collimation and no gantry tilting. Data are then reconstructed as 1-mm thick slices with 50% slice overlap, on the axial plane. This set of images is suitable for excellent MPR post-processing (Table 1.4).

Table 1.4. MSCT scanning parameters

Parameters	MSCT (4 rows)	MSCT (16 rows)
Orientation	Axial, no gantry tilting	
Collimation	4×1 mm	16×0.75 mm
Rotation time	0.75 s	0.75 s
mA/kV	70/133	60/120÷140
Reconstruction algorithm – *kernel**	H70h	H70h
Volume reconstruction (axial plane)		
Thickness	1.25 mm	1 mm
Interslice gap	0.7 mm	0.5 mm

* Siemens equipment

1.3 MR Technique

MR plays a prominent role in imaging of the paranasal sinuses. Its high contrast resolution combined with multiplanar capability make it a valuable tool in the assessment not only of benign and malignant neoplasms, but also in the evaluation of aggressive inflammatory lesions (invasive mycoses, Wegener granulomatosis, sarcoidosis). In these settings, the high contrast resolution of this technique enables discrimination between the lesion and intrasinusal retained secretions, demonstrating its relationships with adjacent structures, and, in many cases, to providing clues for a differential diagnosis. In contrast, no major indication to MR is found for patients affected by chronic rhino sinusitis or nasal polyposis: scant detail relating to thin bone structures (which are numerous and critical in this area) and high costs are substantial drawbacks (Zinreich 1998).

1.3.1 Designing an MR Protocol: Basic Concepts

Though modern equipment enables rapid acquisition of nearly all kind of sequences, a basic principle guides the design of an MR protocol: the faster the examination time, the lower the risk of motion artifacts. A second key point consists in spatial resolution: nasal cavity and paranasal sinuses are a complex framework of airspaces bordered by thin, bony boundaries. Moreover, a thin osteo-periosteal layer separates the sinonasal region from the anterior cranial fossa (cribriform plate and dura) and the orbit (lamina papyracea and periorbita). An adequate depiction of these structures mandates high field equipment (1.5 T) and a dedicated circular coil (head coil). In addition, a high-resolution matrix (512) should be applied along with the smallest FOV achievable (individually variable, but generally 180–200 mm). Smaller FOV may be obtained but this, of course, requires oversampling in the phase encoding direction to avoid aliasing artifacts, and therefore results in an overall increase of examination time. Acquiring images not exceeding 3–3.5 mm thickness, with an interslice gap ranging from 1.5 mm to 2.4 mm (50%–70%) is also recommended. The parameters listed above, applied to both TSE T2 and SE T1 sequences, are an acceptable compromise between the need to attain small pixel size and the risk of significantly decreasing signal-to-noise ratio.

1.3.2.1 MR Protocol

Symmetric representation of anatomic structures is of the utmost importance, as in many cases the diagnosis may be based on the observation of differences in size and signal intensity of a paired structure when matching the two sides. To achieve this, the internal auditory canals, imaged with a TSE T2 localizer sequence, are taken as a landmark to correctly orientate axial and coronal studies. As for CT protocols, the hard palate is a second point for reference for proper sequence orientation (parallel on axial plane, perpendicular on coronal plane); sagittal studies are aligned to the nasal septum and falx cerebri.

The sequences applied are, basically, TSE T2 and SE T1. The first one provides the best discrimination between solid tissue and fluids (retained secretions, cerebrospinal fluid, colliquated tissues). It is acquired in axial plane and in a second perpendicular plane chosen according to the priority dictated by the lesion site of origin and clinical signs (Table 1.5). SE T1 has the advantage of a superior anatomic resolution, valuable for the definition of the interface between lesion and adjacent structures. Moreover,

Table 1.5. Standard MR protocol

Sequence	TR (ms)	Thickness (mm)	Averages	Matrix	Pixel (mm)	Acquisition time
TSE T2	5680	3–3.5	3	512×256	0.8×0.4×3	2'06"
Gd-DTPA SE T1	400	3–3.5	2	512×256	0.7×0.4×3	2'50"
Total examination time	(2 TSE T2 + 3 SE T1) **12'42"**					
Optional sequences						
FS TSE T2	5960	3–3.5	3	512×256	0.8×0.4×3	2'13"
FS Gd-DTPA SE T1	695	3–3.5	2	512×256	0.7×0.4×3	4'53"

in this sequence fat tissue signal is maximized. This issue enables detection of subtle signal changes in the medullary part of bone, as well as to accurately detect the effacement of fat tissue pads, particularly in critical areas such as the orbit and the pterygopalatine fossa. Plain SE T1 sequence has two major indications:

- Patients examined for lesions of unclear etiology. In this case, additional information is provided regarding signal pattern of the lesion, therefore supporting the differential diagnosis task.
- Patients followed up after treatment. In this scenario a plain SE T1 sequence helps to retrospectively assess the enhancement pattern of a suspect lesion, therefore it offers clues to discriminate a recurrent lesion from scar tissue.

After the administration of paramagnetic contrast agent (Gd-DTPA, 0.2 ml/kg body weight), a SE T1 sequence is acquired in all three planes.

Fat-sat prepulses may be applied to both TSE T2 and enhanced SE T1 sequences to increase lesion conspicuity (particularly in malignant tumors) and to delineate the relationships between a lesion and intraorbital/pterygopalatine fat tissue. The main disadvantage on fat-sat TSE T2 sequences is represented by the loss of a natural contrast agent. Fat tissue (suppressed), bone, and muscular structures all display a hypointense signal, resulting in a difficult delineation of the interface between normal and pathologic tissues. On the other hand, post-contrast fat-sat SE T1 requires a considerable increase of repetition time (TR) that influences both T1 weighting of images and acquisition time. These pitfalls may be solved only by decreasing the number of acquired slices and, therefore, the anatomic coverage. As a result, in our experience, fat-sat technique is preferably applied to SE T1 sequences in collaborative patients, focusing on restricted anatomic areas.

1.3.2.2 Additional MR Sequences

Volumetric interpolated breath-hold imaging (VIBE) is a 3D MR technique aimed at minimizing partial volume effects and maximizing image contrast, and represents a robust alternative to SE T1 sequences. This fat-sat gradient-echo T1 weighted sequence has the potential to provide submillimetric sections, no gaps, and isotropic voxels, thus making it suitable for optimal MPR/MIP reconstructions in all planes.

Due to its high flexibility, it can be optimized for *short acquisition times* (slice thickness 0.7 mm, 144 partitions, matrix size 320, acquisition time 1'26") (Table 1.6). When accurate synchronization of contrast injection and image acquisition is fulfilled, the same sequence may provide high-quality MR angiograms, to correctly demonstrate the relationships between tumor and vessels.

Adequate arrangement of parameters (slice thickness 0.5 mm, 224 partitions, matrix size 448, acquisition time 3'52") converts VIBE into a robust high resolution sequence (Fig. 1.1) that allows full coverage of the paranasal sinuses and skull base, valuable for precise definition of tumor extension and perineural spread (Table 1.6).

Table 1.6. VIBE sequence

	Standard VIBE	High resolution VIBE
TR	6.02 ms	818 ms
TE	2.55 ms	3.47 ms
Scan time	1'26"	3'52"
Voxel size	0.7×0.7×0.7 mm	0.5×0.5×0.5 mm
Partitions	144	244
Coverage	100 mm	0.5 mm
FoV read	320 mm	230 mm
Averages	1	1
Image matrix	320×208	448×208

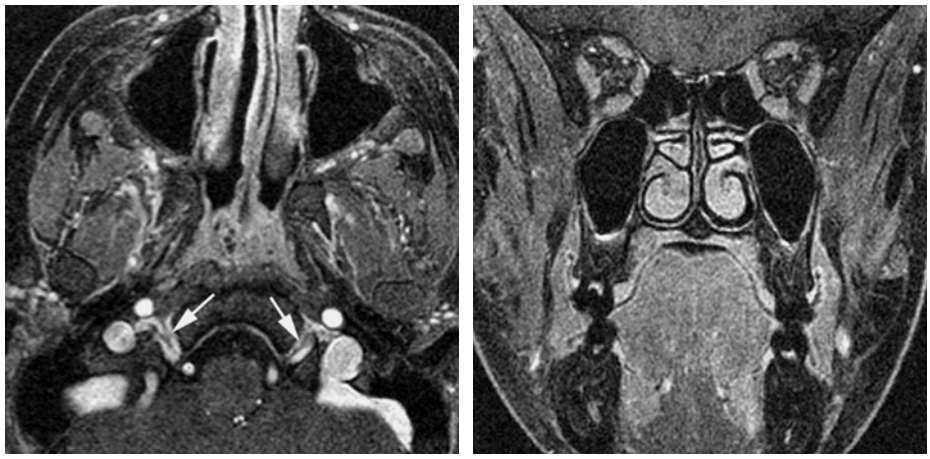

a b

Fig. 1.1a,b. High resolution VIBE sequence (matrix 448×448, acquisition time 3'48") on axial (**a**) and coronal (**b**) planes. Excellent anatomic definition is demonstrated by the identification of the subtle hypointense hypoglossal nerve, as it courses through the condylar canal, surrounded by enhanced veins (*arrows*)

1.3.2.3 Signal vs Time Curves in Follow-Up Studies

After surgery and/or radiation therapy, precise discrimination between scar tissue and recurrent/persistent tumor is often a hard task. An easy and reliable guide for differential diagnosis may be obtained by comparing signal vs time curves of suspected lesions vs normal mucosa, muscle, or vascular structures. This approach requires a dynamic sequence (GE T1), acquiring the same section with a frame rate of 1/s, for 1 min. Signal curves are then calculated by placing regions of interest on the suspect lesion and on adjacent normal tissues (vessels, muscles, mucosa) (Fig. 1.2). Helpful information can be obtained by comparing both the average of maximum signal values and the steepness of the curve, in suspect and presumably normal tissues. The main drawback of this application is represented by its limited coverage: the dynamic sequence acquired allows just a single section to be selected after the acquisition of TSE T2 and plain SE T1 sequence.

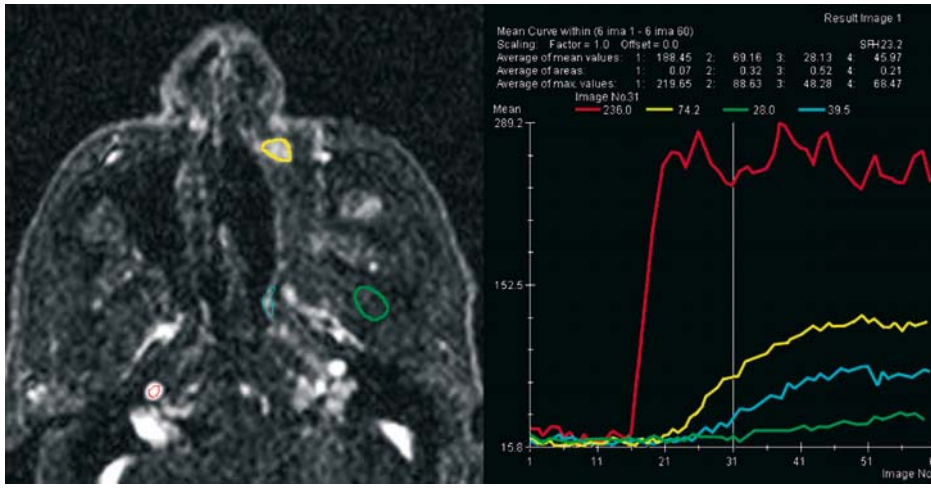

Fig. 1.2. Time versus signal curve. Follow-up MR after radical maxillectomy for adenocarcinoma. Dynamic acquisition (single slice, one scan/s, acquisition time 60 s) after bolus injection of Gd-DTPA. By placing regions of interest on the internal carotid artery (*red*), suspect recurrent tumor (*yellow*), and presumably normal muscle (*green*) and mucosa (*blue*), a time vs signal intensity curve is calculated. Compared to normal tissue, the suspect lesion shows steeper and higher curve. The finding was confirmed at aspiration cytology (true positive)

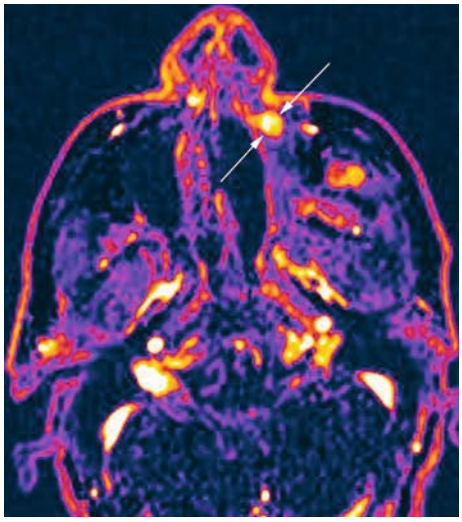

Fig. 1.3. Parametric image obtained from the whole stack of 60 frames. Intensity is related to the slope of the time-enhancement curve. *Arrows* point to the confirmed recurrent tumor

References

Hagtvedt T, Aalokken TM, Notthellen J et al (2003) A new low-dose CT examination compared with standard-dose CT in the diagnosis of acute sinusitis. Eur Radiol 13:976-980

Hein E, Rogalla P, Klingebiel R et al (2002) Low-dose CT of the paranasal sinuses with eye lens protection: effect on image quality and radiation dose. Eur Radiol 12:1693-1696

MacLennan AC (1995) Radiation dose to the lens from coronal CT scanning of the sinuses. Clin Radiol 50:265-267

Maroldi R, Battaglia G, Maculotti P et al (1998) Spiral CT vs subsecond conventional CT in head and neck malignancies. In: Krestin GP, Glazer GM (eds) Advances in CT IV. Springer, Berlin Heidelberg New York, pp 70-75

Oliverio PJ, Benson ML, Zinreich SJ (1995) Update on imaging for functional endoscopic sinus surgery. Otolaryngol Clin North Am 28:585-608

Phillips CD (1997) Current status and new developments in techniques for imaging the nose and sinuses. Otolaryngol Clin North Am 30:371-387

Sievers KW, Greess H, Baum U et al (2000) Paranasal sinuses and nasopharynx CT and MRI. Eur J Radiol 33:185-202

Sohaib SA, Peppercorn PD, Horrocks JA et al (2001) The effect of decreasing mAs on image quality and patient dose in sinus CT. Br J Radiol 74:157-161

Zammit-Maempel I (1996) Radiation dose to the lens from coronal CT scanning of the sinuses. Clin Radiol 51:151

Zammit-Maempel I, Chadwick CL, Willis SP (2003) Radiation dose to the lens of eye and thyroid gland in paranasal sinus multislice CT. Br J Radiol 76:418-420

Zinreich SJ (1998) Functional anatomy and computed tomography imaging of the paranasal sinuses. Am J Med Sci 316:2-12

2 CT and MR Anatomy of Paranasal Sinuses: Key Elements

Roberto Maroldi, Andrea Borghesi, Patrizia Maculotti

CONTENTS

2.1 Introduction

A conceptual understanding of the anatomic and functional relationships between the nasal cavity and paranasal sinuses is of the utmost importance, particularly when dealing with chronic inflammatory diseases.

According to their drainage pathway, the sinusal cavities may be functionally classified into two subgroups. The first one includes the anterior ethmoid cells, the frontal sinus, and the maxillary sinus; all these cavities drain mucus into the middle meatus. The second group encompasses the posterior ethmoid cells and the sphenoid sinus, both draining into the superior meatus.

R. Maroldi, MD
Professor, Department of Radiology, University of Brescia, Piazzale Spedali Civili 1, Brescia, BS, 25123, Italy
A. Borghesi, MD; P. Maculotti, MD
Department of Radiology, University of Brescia, Piazzale Spedali Civili 1, Brescia, BS, 25123, Italy

2.1.1 Nasal Cavity and Lateral Nasal Wall

Nasal cavities are located in the midface, separated by a median septum; they communicate posteriorly with the nasopharynx through the choanae. The floor of nasal fossae is the hard palate, the cribriform plate and the planum ethmoidalis compose its roof, that separate nasal cavities from the anterior cranial fossa. The nasal septum is made of a "hard" portion (perpendicular lamina of the ethmoid, vomer), and of a "soft" part (septal cartilage).

The lateral nasal wall has a more difficult anatomy, an understanding of it being critical for endonasal surgery planning.

The complex anatomical arrangement of the lateral nasal wall can be more easily understood if related to the embryologic development of turbinates and ethmoid (Wolf et al. 1993).

The ethmoid turbinates originate from ridges in the lateral nasal wall of the fetus. Each of the five ridges (ethmoidoturbinals) has an ascending (more vertical) and descending (more horizontal) portion, being – therefore – similar to the turbinate in the adult. Between the fetal ridges are six grooves. Some ridges and grooves will fuse or disappear – partially or totally – during fetal development to ultimately result in the nasal turbinates of the adult. Key points are:

The first ethmoidoturbinal regresses, i.e. will not develop into a turbinate. The agger nasi is considered a residual of the ascending portion, while the uncinate process is presumably a remnant of the descending portion.

The descending part of the first groove (located between the first and second ethmoidoturbinals) becomes the ethmoidal infundibulum and middle meatus, whereas the ascending part becomes the frontal recess.

The second ethmoidoturbinal gives rise to the bulla lamella, a lamina attached to the lateral nasal wall, a structure that can be observed in few patients because it is usually pneumatized, therefore appearing as the bulla ethmoidalis.

The third and fourth ethmoidoturbinals develop, respectively, into the permanent middle and superior turbinates; and the fifth ethmoidoturbinals become the supreme (uppermost) turbinate.

The superior and uppermost meatus develop from third and fourth fetal grooves.

As a result, ridges fully develop into thin laminae crossing the entire ethmoid to project into the nasal cavity (turbinates) or give rise to incomplete laminae, like the uncinate process. Each bony lamina has a constant portion inserting into the lateral nasal wall (ground lamella) and additional attachments to the lamina cribrosa or to the fovea ethmoidalis (superiorly).

In most subjects, four ground lamellae are usually present, almost each one obliquely oriented, somewhat parallel to one another. The uncinate process – an incompletely developed lamella – is the first one, followed by the bulla lamella. If the latter extends vertically up to the ethmoid roof, the frontal recess becomes separated from the rest of the ethmoid. Pneumatization of this lamella results in the development of the ethmoidal bulla. The third, more constant and complete ground lamella consists of the lateral insertion of the middle turbinate on the lamina papyracea. This lamella separates anterior from posterior ethmoidal cells. A fourth lamella is made by the lateral attachment of the superior turbinate. Occasionally, a fifth lamella may be observed when the supreme turbinate does not regress (Kim et al. 2001).

The spaces among the ground lamellae (interturbinal meatus) are further subdivided by transverse bony septa, resulting in several cells that communicate with the interturbinal meatus only through a small ostium. Rarely these septa are absent. In this latter condition, the original framework of the labyrinth organized into single large cells – corresponding to the interturbinal meatus – can be observed.

Variations or anomalies in the development of ground lamellae and septa will result in a great variability of number, size and morphology of the single ethmoid cells and may additionally reflect on the ratio between the volume of anterior versus posterior cells.

As mentioned above, the *superior meatus* is the drainage pathway of posterior ethmoid cells and sphenoid sinus (the latter through the sphenoethmoid recess).

The middle meatus plays a crucial functional role, as in this area the secretions of several sinuses are collected, namely:

- The ethmoid bulla (roof of the meatus)
- The anterior ethmoid cells and maxillary sinus, both through the hiatus semilunaris, a subtle fissure located in front and below the ethmoid bulla
- The frontal sinus, through the frontal recess

The inferior meatus, although the largest, has a less relevant functional role: in this space only the distal opening of the nasolacrimal duct is found.

2.1.2 Ethmoid Bone

From a practical standpoint, the ethmoid bone can be divided into four structures: two lateral masses, a sagittal midline lamina, and a horizontal plate (Fig. 2.1). The latter (cribriform plate) is the central part of the floor of the anterior cranial fossa. Several microscopic foramina perforate its thin structure, through which course the olfactory nerve filaments with their perineural investment.

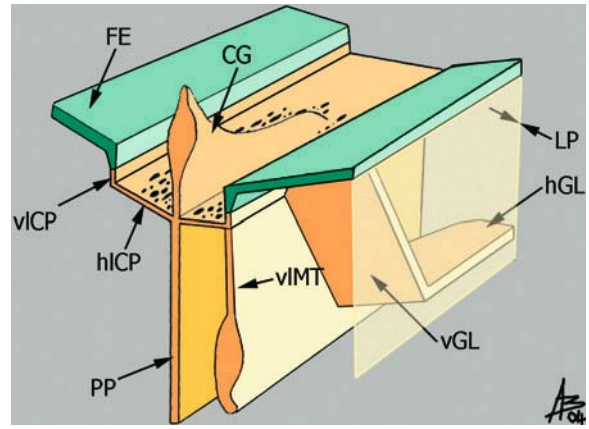

Fig. 2.1. The ethmoid plates and fovea ethmoidalis. A midline (perpendicular plate, *PP*) and two lateral vertical laminae: the medial one made by the vertical lamella of the middle turbinate (*vlMT*) on the top of which is the vertical lamella of the cribriform plate (*vlCP*), the lateral one is the lamina papyracea (*LP*). Horizontal lamella of the cribriform plate (*hlCP*), horizontal (*hGL*) and vertical (*vGL*) – ascending part – of ground lamella of the middle turbinate, crista galli (*CG*), fovea ethmadalis (*FE*)

On the upper part of the sagittal midline lamina (crista galli) – located just above the cribriform plate – inserts the cerebral falx; the inferior part, below the cribriform plate, being referred to as the perpendicular lamina, a component of the nasal septum (Fig. 2.2–2.4).

The lateral masses (ethmoid labyrinth) are made of a variable number (3–18) of pneumatized cells separated by thin bony walls.

Each ethmoid labyrinth is closed by bony margins on its external and internal surfaces only. The

external surface is made by the lamina papyracea that separates the cells from the orbit. Dehiscences may be present. As a result, the periosteum of the ethmoid cell comes in contact with the periosteum investing the orbital wall (periorbita). Medially, the labyrinth is bordered by two constant laminae hanging from the horizontal plate: the middle and superior turbinates. An uppermost small third ethmoid turbinate (supreme turbinate) can seldom be observed.

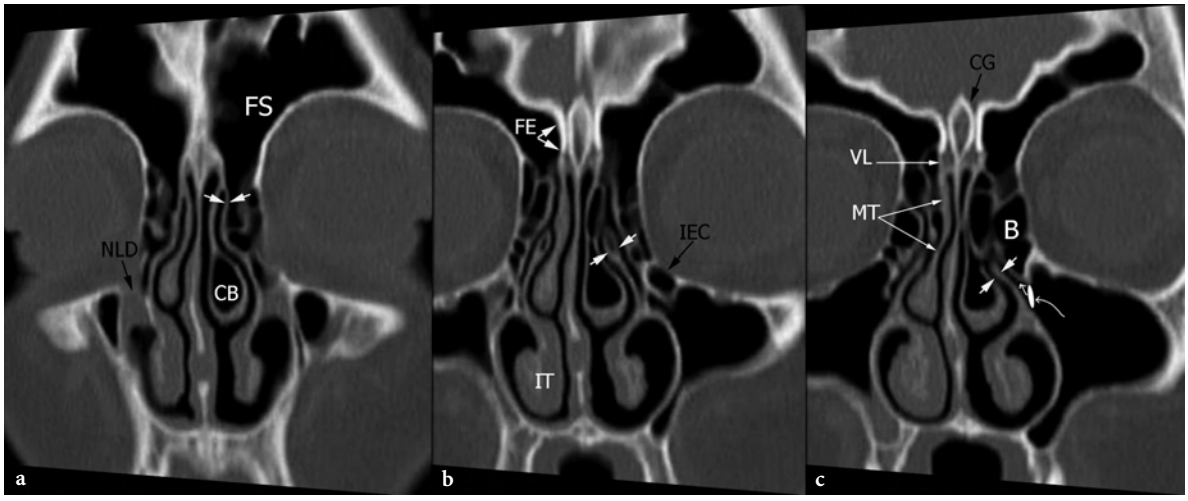

Fig. 2.2a–c. CT coronal reconstructions through the ethmoid labyrinth. **a** Anterior nasal fossa, level of the uppermost insertion of both uncinate processes on the vertical lamellae of the middle turbinates – type 4 according to Landsberg and Friedman (2001) (*white arrows* on *left side*). **b** Bilateral pneumatization of the horizontal (non-attached) free portion of the uncinate processes (*white arrows* on *left side*). **c** The horizontal portion of the uncinate process (*white arrows* on *left side*) and the inferior surface of the ethmoid bulla (*B*) limit the oblique and narrow ethmoid infundibulum. The maxillary sinus ostium is detectable at the bottom of the infundibulum (*white ellipse*). *Curved white arrows* show the path along the ostium and the infundibulum

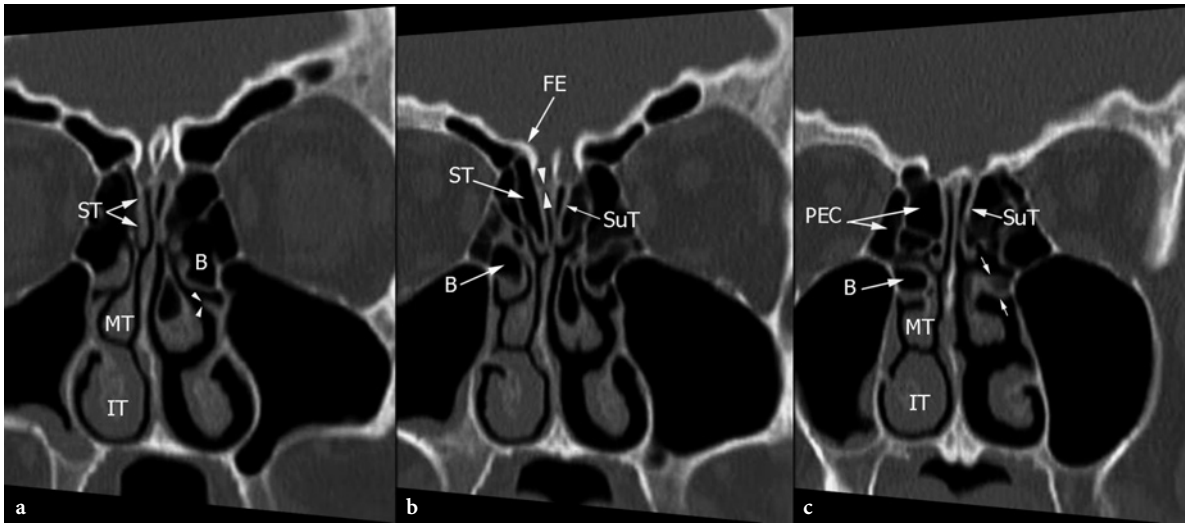

Fig. 2.3a–c. CT coronal reconstructions through the ethmoid labyrinth. **a** Middle nasal fossa at the level of the short horizontal portion of the uncinate process posterior to the ethmoid infundibulum (*white arrowheads* on *left side*). A large ethmoid bulla (*B*) impinges the left middle turbinate on left side. **b** The CT section cuts the posterior part of the bulla (*B*). The horizontal portion of the cribriform plates (*arrowheads*) appears thinner than the bone of the fovea ethmoidalis (*FE*). Bilateral pneumatization of the superior turbinate (*ST*) is present. **c** Lateral attachment of the middle turbinate – the ground lamella (*opposite arrows*) – onto the lateral nasal wall. Posterior ethmoid cells (*PEC*) extend between the lamina papyracea and the supreme turbinate (*SuT*)

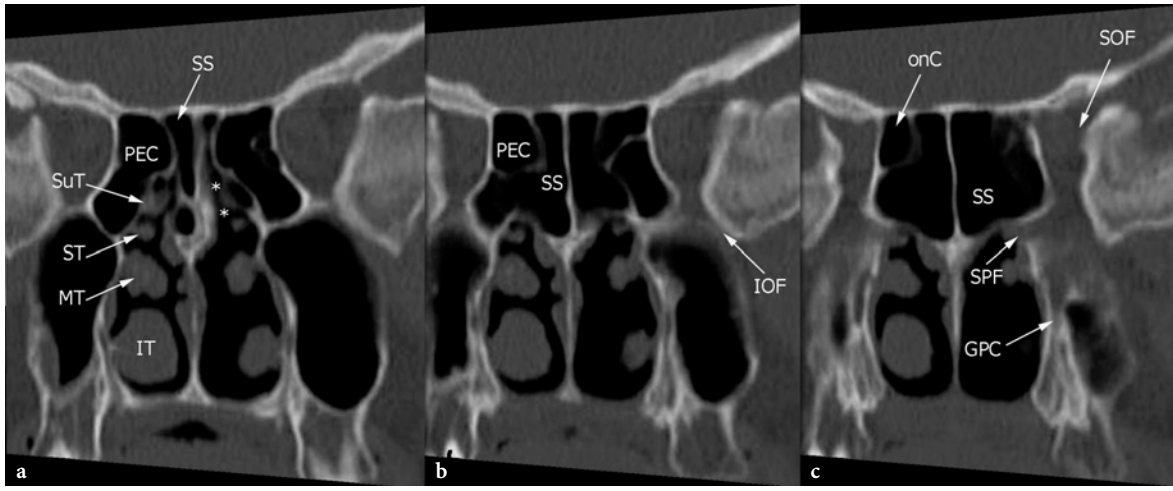

Fig. 2.4a–c. CT coronal reconstructions through the posterior ethmoid labyrinth and the sphenoid sinus. **a** Level of the sphenoethmoid recess (*asterisks*). Lateral attachment of all four turbinates (*IT*, *MT*, *ST*, and *SuT*) is shown. Anterior aspect of the sphenoid sinus (*SS*) and posterior ethmoid cells (*PEC*) are demonstrated on the same level. A posterior ethmoid cell extends over the right sphenoid sinus – Onodi cell (*onC*) on (**b**) and (**c**). Inferior orbital fissure (*IOF*), superior orbital fissure (*SOF*), sphenopalatine foramen (*SPF*), greater palatine canal (*GPC*)

The middle turbinate – the largest ethmoid lamina – separates the labyrinth into anterior and posterior cells by means of its middle portion inserting on the lateral nasal wall (ground lamella) (Fig. 2.5).

All the other surfaces of the labyrinth are open, lined only by adjacent structures. Anteriorly, cells open into a narrow cleft – the infundibulum ethmoidalis – that empties into the nasal cavity through the middle meatus. On the opposite surface, the anterior aspect of the sphenoid sinus borders the posterior ethmoid cells, that empty into another narrow cleft – the sphenoethmoidal recess – draining into the superior meatus and finally into the choanae.

The orbital plate of the frontal bone (fovea ethmoidalis) provides the bony roof of the ethmoid as the cells within the labyrinth extend above the plane of the cribriform plate (Lebowitz et al. 2001). The transition between the thicker frontal bone and the thinner, medially located, lateral lamella of the lamina cribrosa can be easily demonstrated on coronal CT planes (Fig. 2.2). The lateral lamella and the lamina cribrosa provide, respectively, the lateral border and the floor of the olfactory fossa. It is important to note that the variability of pneumatization of the labyrinth reflects not only on the height of the lateral lamella – therefore the relative depth of the olfactory fossa into the nasal cavity – but also on its obliquity and on the transverse size of the lamina cribrosa. Relevant side to side variations are frequently observed.

Moreover, the weakest area of the whole anterior skull base is located where the anterior ethmoidal artery enters the lateral lamella after having crossed the lamina papyracea and the ethmoidal labyrinth. On CT, this area can be detected as a focal, sometimes symmetrical, dehiscence on the lateral lamella of the lamina cribrosa.

2.1.3 Frontal Sinus and Frontal Recess

Anterior pneumatization of the frontal recess into the frontal bone gives rise to the frontal sinus (Fig. 2.6). In the sagittal plane its ostium can be identified as the narrowest part of an hourglass space, the upper part widening into the frontal sinus, and the lower emptying into the middle meatus through the frontal recess. The latter is not a true tubular structure, as the term "nasofrontal duct" might indicate. In effect, the size and shape of the frontal recess are largely dictated by the adjacent structures: the agger nasi cells anteriorly, the ethmoidal bulla posteriorly, the vertical portion of the uncinate process and the middle turbinate on medial and lateral aspects (Fig. 2.7).

Particularly, the medial and lateral borders of the frontal recess depend on the variable type of the superior attachment of the uncinate process. Six variations have been identified by Landsberg and Friedman (2001) (Fig. 2.8). In type 1, insertion on lamina papy-

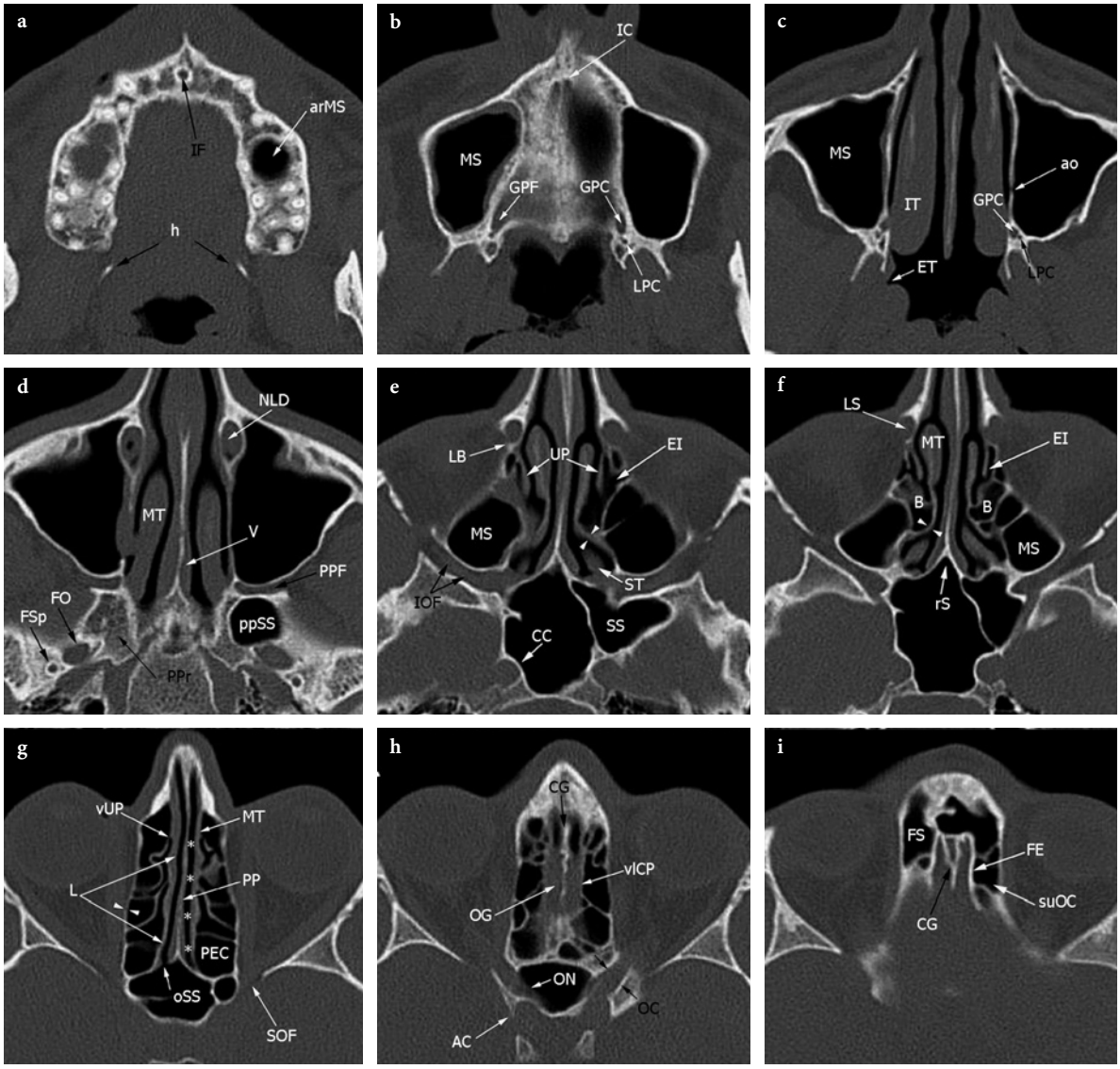

Fig. 2.5a–i. Axial plane. **a** Level of the alveolar process, teeth roots are seen. The inferior portion of medial pterygoid plates – hamulus – is detected (*h*). Alveolar recess of maxillary sinus (*arMS*) **b** Hard palate level. Greater (*GPC*) and lesser (*LPC*) palatine canals result from the articulation of the vertical portion of the perpendicular plate of the palatine bone with the maxillary bone. Opening of the canal – the greater palatine foramen (*GPF*) – appears as an ovoid groove on the *right side*. **c** The inferior concha and the surrounding inferior turbinate (*IT*) are demonstrated. An accessory ostium is located within the posterior third of the medial maxillary sinus wall (*ao*). **d** Level of the inferior aspect of the nasolacrimal ducts (*NLD*). The postero-superior limit of the middle turbinates reaches the choanae (*MT*). **e** Level of the middle meatus. The uncinate processes (*UP*) attach onto the medial aspect of the NLD. The narrow space between the UP and the medial maxillary sinus wall belongs to the ethmoid infundibulum (*EI*). *Arrowheads* indicate the ground lamella of the MT, signing the border between anterior and posterior ethmoid labyrinth (see also **f**), into which the inferior tip of the superior turbinates (*ST*) projects. **f** The ethmoid bullae (*B*) border the posterior limit of the EI. Rostrum of the sphenoid bone (*rs*). **g** The vertical portion of the UP (*vUP*) attaches onto the vertical lamellae of the MT on both sides. A clear separation between anterior and posterior ethmoid cells (*PEC*) cannot be identified on axial planes. The narrow channel-like olfactory fissure (*asterisks*) reach the sphenoethmoidal recess where the ostium of the right sphenoid sinus appears as a small opening close to the midline (*oSS*). Common lamina onto which the middle, superior (and supreme) turbinates attach (*L*). *Arrowheads* indicate the thin lamina papyracea. **h** Olfactory groove (*OG*) level. Because the groove extends down into the labyrinth, it results bordered by ethmoid cells. The thin vertical lamella of the cribriform plate (*vlCP*) separates the groove from the ethmoid cells. **i** At the level of the mid crista galli (*CG*) the olfactory groove is bordered laterally by the thicker frontal bone – fovea ethmoidalis (*FE*). *suOC*, supraorbital ethmoid cell

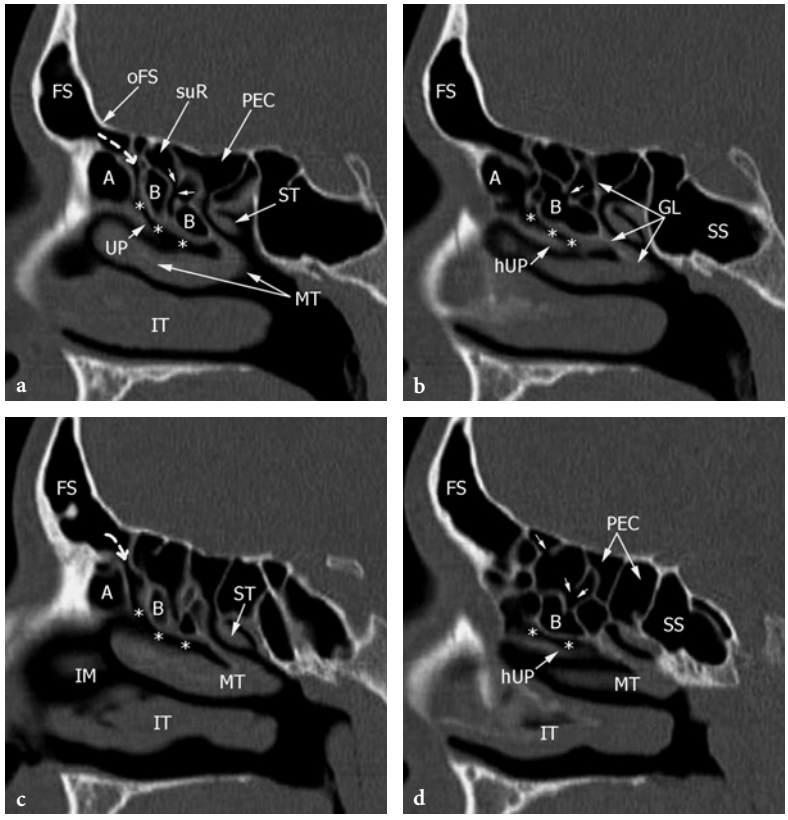

Fig. 2.6a–d. Same patient as in Fig. 2.5. **a,b** Right side. **c,d** Left side. **a** Sagittal plane closer to midline. From the hourglass ostium of the frontal sinus (*oFS*) the mucus follows a curved path (*broken curved arrow*) into the frontal recess between the agger nasi cell (*A*) and the anterior surface of the bulla (*B*). *Asterisks* on (**a**) and (**b**) indicate the course of the hiatus semilunaris bordered by the uncinate process – horizontal (*hUP*) and part of the vertical portion – and the bulla. *suR*, suprabullar recess. **c** Sagittal plane closer to midline. The left frontal sinus ostium is wider than on the opposite side. Because the agger nasi cell (*A*) is smaller, the frontal recess is more vertically oriented (*broken curved arrow*). **d** On a more lateral plane the horizontal portion of the uncinate process is demonstrated (*hUP*). *Asterisks* indicate the hiatus semilunaris. *Small arrows* on (**a**)/(**b**) and (**d**) point to the opening of small anterior ethmoid cells into the bulla ethmoidalis

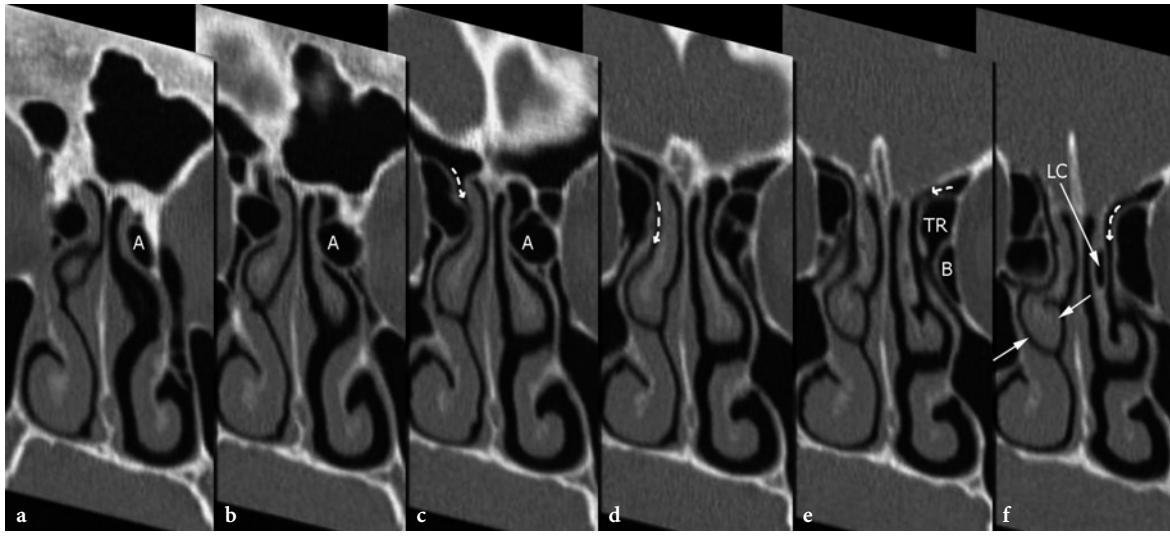

Fig. 2.7a–f. The left vertical portion of the uncinate process inserts on both the lateral surface of a large agger nasi cell (*A*) and the lamina papyracea. As a result, the frontal recess runs medial to the uncinate process (*broken curved white arrows*). Moreover, a terminal recess (*TR*) is created between the superior surface of the bulla and the insertion of the UP onto the lamina papyracea. On coronal scans the agger nasi cell may be differentiated from the bulla ethmoidalis because it is located anterior to the infundibulum ethmoidalis. On the *right side*, a large bulla is associated with a paradoxically curved middle turbinate (*opposite arrows*). Pneumatization of the vertical lamella of left middle turbinate (lamellar concha, *LC*)

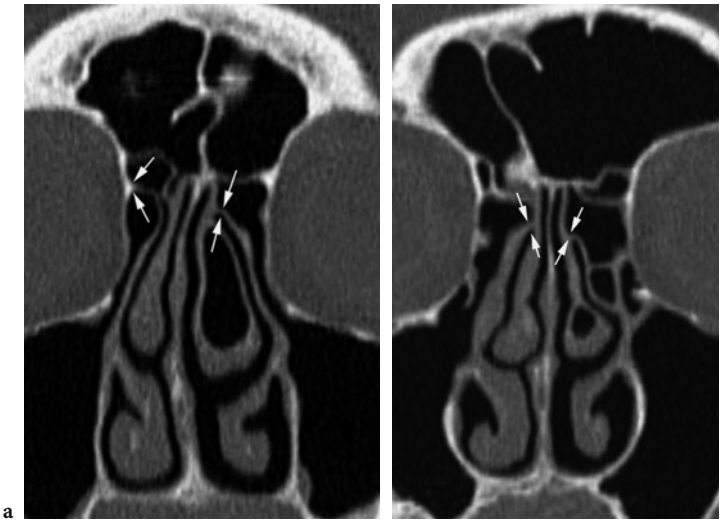

a b

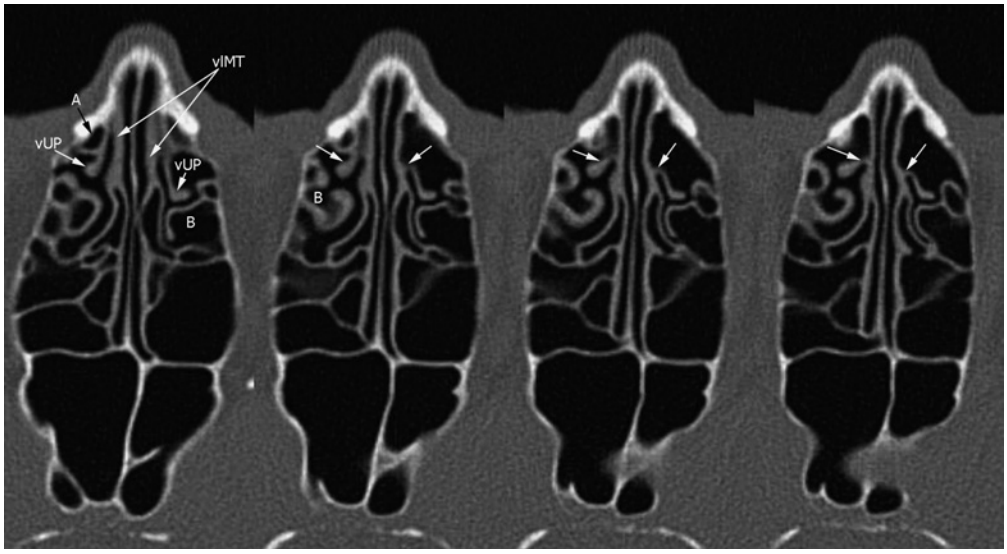

c

Fig. 2.8a–c. **a** The vertical portion of the uncinate process inserts onto the lamina papyracea [type 1, according to Landsberg and Friedman (2001)] – right side – and onto the upper aspect of middle turbinate (type 6) – left side. **b** Bilateral insertion of the uncinate process onto the lateral aspect of the middle turbinate. **c** Same patient as in (**b**). The vertical portion of both uncinate processes (*vUP*) reaches the vertical lamella (*vlMT*) of the middle turbinates

racea, and type 2, insertion on the posteromedial wall of agger nasi cells, the middle turbinate serves as the medial border of the recess and the uppermost uncinate process provides its lateral limit. In type 3, a double insertion – to lamina papyracea (anteriorly) and to the junction of middle turbinate on cribriform plate (posteriorly) – is present. In type 4–6 – insertion to the junction of middle turbinate with the cribriform plate, to the fovea, to the middle turbinate, respectively – the uppermost uncinate process becomes the medial border of the recess, the bulla and lamina papyracea being the lateral limit.

As a result, the frontal recess may empty medial to the uncinate process being separated from the ethmoidal infundibulum (type 1–3), or it may run laterally to the uncinate and join the ethmoidal infundibulum (type 4–6).

Because the frontal recess is bordered, anteriorly, by the agger nasi cells, its width on the sagittal plane depends on the extent of their pneumatization (Fig. 2.6). Furthermore, the posterior border may also vary: it is formed by a single and continuous bony wall when the ground lamella of the bulla ethmoidalis reaches the ethmoid roof. Otherwise, when the ground lamella of the bulla does not insert on the skull base, the frontal recess communicates with a narrow space (sinus lateralis or retrobullar recess) extending above (suprabullar recess cell) and behind the bulla, posteriorly bordered by the ground lamella of the middle turbinate.

Anterior ethmoidal cells developed from the frontal recess may extend into the frontal sinus itself (bulla frontalis), making it rather difficult to distinguish the true frontal sinus from a bulla frontalis cell. Frontal

cells have been defined by Bent et al. (1994) to derive from the anterior ethmoid sinus behind the agger nasi and to pneumatize the frontal recess above the agger nasi. Four types have been recognized: a single or several – a tier – frontal cell(s) located over the agger nasi identify type 1, and type 2, respectively. A single large cell extending cephalad into the frontal sinus belongs to type 3. Type 4 identifies a single isolated cell within the frontal sinus (Figs. 2.9–2.11). If not properly identified on a pre-surgical CT examination, the frontal cells type 3 and 4 may be mixed up for the real frontal sinus, potentially resulting in an incorrect procedure.

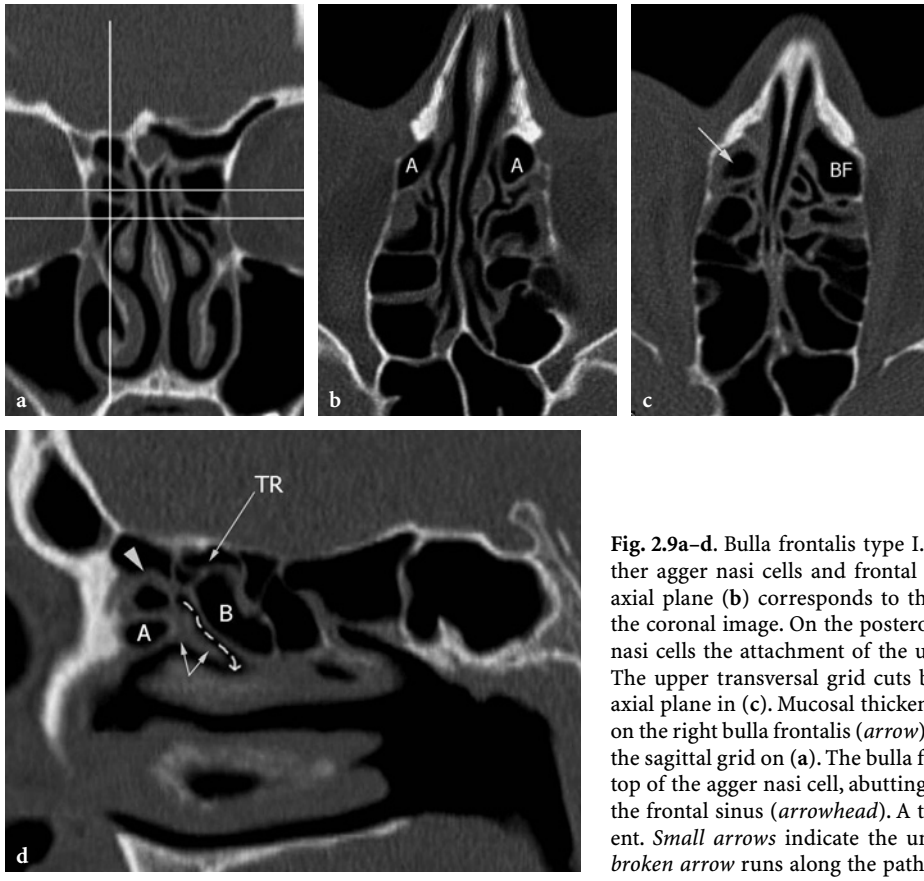

Fig. 2.9a–d. Bulla frontalis type I. **a** On the coronal image either agger nasi cells and frontal cells type I are shown. The axial plane (**b**) corresponds to the lower transversal grid on the coronal image. On the postero-medial aspect of the agger nasi cells the attachment of the uncinate processes is visible. The upper transversal grid cuts both frontal cells giving the axial plane in (**c**). Mucosal thickening on the internal surfaces on the right bulla frontalis (*arrow*). **d** The plane corresponds to the sagittal grid on (**a**). The bulla frontalis type I locates on the top of the agger nasi cell, abutting its roof and projecting into the frontal sinus (*arrowhead*). A terminal recess (*TR*) is present. *Small arrows* indicate the uncinate process. The *curved broken arrow* runs along the path of the frontal recess

Fig. 2.10. Bilateral bulla frontalis, chronic sinusitis. A tier of several small frontal bullae – type II – is demonstrated on the *right side* (*black arrows*). Air has been replaced by fluid within bullae and frontal sinus (*FS*). A large bulla frontalis on the *left* (type III) is also detected (*white arrows*)

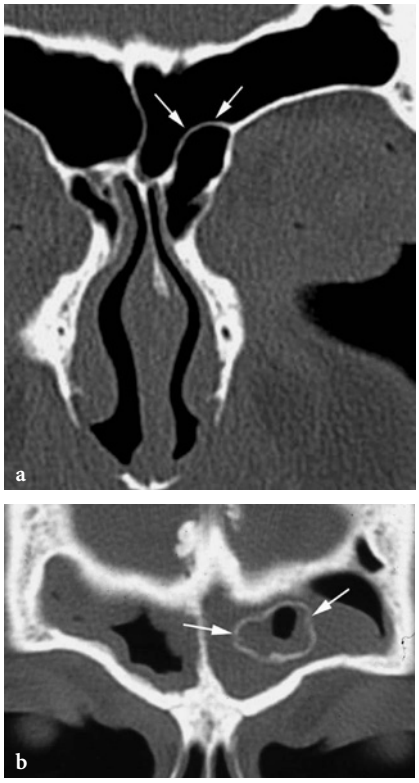

Fig. 2.11. **a** A large bulla frontalis type III projects into the right frontal sinus (*arrows*). **b** Demonstration of an isolated frontal cell type IV (*arrows*) with mucosal thickening inside (and within surrounding frontal sinusal walls)

2.1.4
Maxillary Sinus, Uncinate Process and Ethmoidal Infundibulum

Maxillary sinuses are the largest sinonasal cavities, bordered by four bony walls. On the anterior wall the distal opening of the infraorbital canal is found. This canal, through which the terminal branch of maxillary nerve courses (infraorbital nerve), is enclosed within the maxillary sinus roof. The infratemporal wall, which is the thinnest and most fragile, separates the maxillary sinus from the pterygopalatine fossa and masticator space, posteriorly.

The medial wall is more complex, it has a natural ostium (Figs. 2.2, 2.12) towards which mucus is actively transported by cilia, and some accessory ostia, normally bypassed by secretions, located either anteriorly and posteriorly to the maxillary ostium (anterior and posterior fontanellae) (Fig. 2.5). Because the horizontal portion (the fetal descending part) of the uncinate process inserts on the medial wall, the maxillary ostium does not directly communicate with the nasal fossa. Conversely, its ostium opens into the floor of a narrow space – i.e. the inferior aspect of the ethmoidal infundibulum (Fig. 2.12). To arrive into the middle meatus, secretions are transported upward along the ethmoidal infundibulum to reach the hiatus semilunaris, a horizontal 2D plane located between the anterior surface of the bulla ethmoidalis and the free margin of the unci-

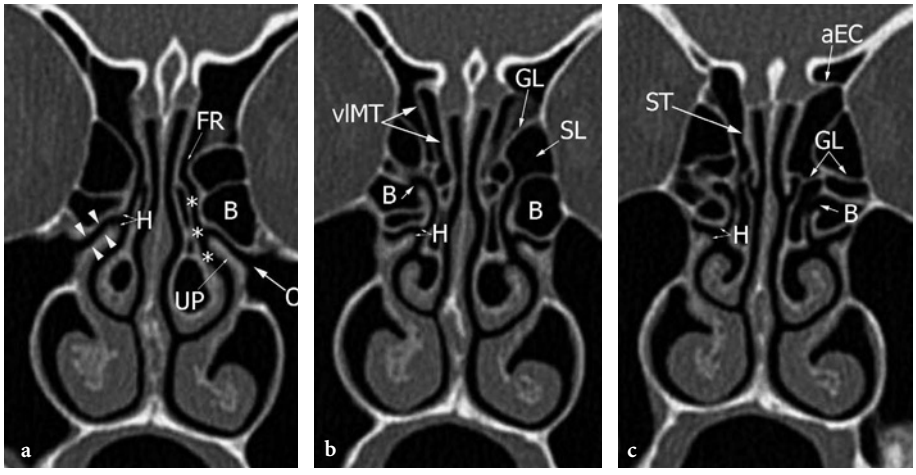

Fig. 2.12a–c. The coronal planes through anterior ethmoid sinus show the different components of the OMU. **a** The maxillary sinus ostium (*O*) communicates with the ethmoid infundibulum (*arrowheads* on *right side*). Ethmoid bulla (*B*) and uncinate process (*UP*) border the infundibulum. The air space between the bulla and the horizontal portion of the uncinate process is part of the hiatus semilunaris (*H*). Frontal recess (*FR*), ethmoid infundibulum and a more posterior opening of the bulla, small arrows on (**b**) and (**c**) open into the middle meatus (*asterisks*). **b** The air space between the attachment of middle turbinate onto the lamina papyracea (ground lamella, *GL*) and the posterior surface of the bulla is the sinus lateralis (*SL*). Pneumatized vertical lamella of the middle turbinate (*vlMT*), superior turbinate (*ST*), anterior canal of the ethmoid (*aEC*)

nate process (Fig. 2.6). The ethmoidal infundibulum is closed anteriorly by the vertical insertion of the uncinate process at the medial maxillary wall, generally forming a sharp angle onto the nasolacrimal duct bony wall (Fig. 2.5). Laterally, the upper portion of the ethmoidal infundibulum is bordered by the lamina papyracea, posteriorly by the ethmoidal bulla. The infundibulum may directly communicate with or be totally separated from the frontal recess depending on the configuration of the uncinate process (see Sect. 2.1.3).

2.1.5 Sphenoid Sinus

Two sinuses, separated by a bony septum that most often lies off the midline, pneumatize the body of sphenoid bone. Septations are frequently demonstrated within the cavities, they are all vertically oriented. Horizontal bony lamellae demonstrated on coronal CT scans belong to posterior ethmoid cells projecting toward or above the sphenoid sinuses. The ostium of sphenoid sinuses is located on the anterior wall, on their superior and medial aspect (Fig. 2.5). It communicates with the sphenoethmoidal recess and the posterior portion of the superior meatus. The sphenoid sinuses are strictly adjacent to relevant anatomic landmarks such as the superior orbital fissure, the optic canal, the cavernous sinus, and the internal carotid artery, laterally; the vault of nasopharynx, below; the hypophysis, above (Fig. 2.1–2.3).

2.2 Development of Nasosinusal Cavities

The size and shape of paranasal sinuses in infants and children differ from those of the adults, resulting in peculiar clinical entities and making surgery more difficult. Their development is linked with the development of the skull and with dentition (Anderhuber et al. 1992).

In the newborn only the ethmoid cells – with the uncinate process, ethmoidal bulla, and hiatus semilunaris – are well developed. They are separated by thick connective tissue that progressively reduces as the cells enlarge, resulting in thin bony septa in the adult. The maxillary sinus is just a shallow sac in the lateral nasal wall, the frontal and sphenoid sinuses are blind sacs only, that have not yet reached the frontal and sphenoid cartilage or bone. The turbinates are well developed and bulky. A superior turbinate is demonstrated in more than 80% of specimens. All nasal meatus are very narrow, causing the newborn to breath through the common nasal meatus.

Between 1–4 years of age, the ethmoid sinus expands in all directions, appearing well developed compared to the other sinuses. The maxillary sinus extends laterally to the infraorbital canal, and caudally to the attachment of the inferior turbinate (Wolf et al. 1993). The frontal and sphenoid sinuses are going to start bone pneumatization, their size being still very small.

Between 4–8 years of age, the ethmoid cells expand more slowly than the frontal and maxillary sinuses. At the age of 7 the frontal sinus extends both medially and laterally into the frontal bone, and the maxillary sinus descends to the middle of the inferior meatus. There are two potentially dangerous situations due to the peculiar anatomy at this age: the uncinate process is close to the medial orbital wall, and the floor of the nose and the floor of the maxillary sinuses are still located at different levels. Uncinate removal is therefore associated with a higher risk of penetrating the lamina papyracea, likewise any attempt to enter the maxillary sinus from the inferior meatus may fail or cause damage of tooth buds.

Between 8–12 years of age, the pneumatization of paranasal sinuses resumes a faster pace. The ethmoid cells are completely developed, and any connective tissue is separating the cells. Due to the eruption of secondary dentition, the maxillary sinus expands causing the choanae to change from circular to rectangular.

Between 12 and 14 years of age, the maxillary sinus reaches the level of the floor of the nasal cavity, and extends to the zygomatic recess, laterally, and to the nasolacrimal duct, medially. The pneumatization of paranasal cavities is almost completed. The sphenoid sinus will reach its permanent size approximately at the age of 22 or 24.

2.3 Surgical Anatomy

Three anatomic areas, corresponding to the narrowest tracts of drainage pathways, are crucial for endoscopic surgery planning: the ostiomeatal (OMU), the frontal recess, and the sphenoethmoid recess.

The OMU is the crossroads of anterior ethmoid, frontal sinus and maxillary sinus mucus transport. This functional unit includes the ethmoidal infundibulum, the maxillary sinus ostium, the ethmoidal bulla, and the uncinate process (Fig. 2.12). The vertical portion of the uncinate process is the real key structure of OMU

because its shape and upper attachment determine the morphology of both the ethmoidal infundibulum and the frontal recess.

The ethmoidal infundibulum is the air passage that connects the maxillary sinus ostium to the middle meatus. To simplify, it can be subdivided into two different portions. The anterior part is the air space located between the vertical portion of the uncinate and the anterior surface of the bulla; whereas the posterior part is the air space situated between the horizontal portion (free, unattached portion) of the uncinate process and the inferomedial surface of the bulla or of the orbit, if the sinus lateralis is present. The gap between the ethmoid bulla and the free edge of the uncinate process is the hiatus semilunaris (Fig. 2.6).

The ethmoid bulla is an important surgical landmark: this is actually the most posterior cell in the anterior ethmoid, protruding in the middle meatus. Its size and morphology are highly variable. The middle turbinate is the medial border of the OMU. This subtle, curved bony structure describes a lateral concavity; it has a cranial anchorage on the cribriform plate – through its vertical lamina – and a lateral insertion on the posterior part of lamina papyracea – through its fan-shaped ground lamella.

The width, path, and morphology of the frontal recess are largely determined by the shape and relationships of the upper part of the uncinate process (type 1–6, see Sect. 2.1.3) and by the variable size and pneumatization of adjacent structures, particularly the ethmoid bulla and agger nasi cells.

Moreover, even the configuration of the ethmoidal infundibulum – and its relationship to the frontal recess depend on the anatomy of the uncinate process (Landsberg and Friedman 2001). In most subjects (up to 52%) its lateral insertion on the lamina papyracea (type 1) creates a "roof" that closes the ethmoidal infundibulum in a blind upper pouch (terminal recess) (Fig. 2.7). If the uncinate process attaches anteriorly to the agger nasi cells (type 2, 18%) the ethmoidal infundibulum is closed superiorly by the floor of the agger nasi. In both configurations, the frontal recess and the ethmoidal infundibulum are separated, and the opening of the frontal recess into the middle meatus is medial to the ethmoidal infundibulum, between the uncinate process and the middle turbinate (Fig. 2.7). As in about 17% of subjects (type 3) the upper part of the uncinate process inserts on both the lamina papyracea and the junction of the middle turbinate with the lamina cribrosa, the frontal sinus opens into the middle meatus in approximately 88% of cases (type 1–3). Conversely, if the uncinate process maintains its complete and longest fetal attachment on the ethmoid roof or medially on the middle turbinate, the frontal recess empties directly into the ethmoid infundibulum, therefore laterally to the uncinate process (Figs. 2.2, 2.8).

From a surgical standpoint, the correct assessment of the frontal recess opening is essential in planning the proper endonasal approach to the frontal recess and the adequate exposure of the frontal sinus. In fact, if the frontal recess opens laterally to the uncinate process, an attempt to find the recess medially to the uncinate would potentially lead toward the olfactory fossa or the frontal lobe.

Because the anterior and uppermost segment of the uncinate process runs obliquely from posterior-inferior to anterior-superior, direct coronal CT scans – obtained perpendicularly to the hard palate – usually do not demonstrate its full course and upper insertion. Multislice CT reconstructions obtained on an oblique plane running along the recess's axis enable a depiction of the actual extent (and insertion) of the unainale process.

The sphenoethmoid recess is outlined by the anterior sphenoid wall and by the posterior wall of posterior ethmoid cells. It conveys sphenoid sinus secretions in the superior meatus (Fig. 2.5).

2.4 Anatomic Variants

Anatomic variants of the OMU structures are relatively frequent; they can be classified as anomalies of size, shape, orientation and entity of pneumatization. In some cases they may impair the physiologic mucous drainage and condition the endoscopic approach. Nevertheless, it must be emphasized that the presence of an anatomic variant does not necessarily imply an increased risk of inflammatory lesion: actually, no direct correlation between anatomic anomalies and nasal obstruction has been clearly demonstrated.

2.4.1 Nasal Septum and Middle Turbinate

Nasal septum deviation is quite a common condition, with its prevalence in asymptomatic subjects reported to range from 20% to 30%; it is usually congenital but may be post-traumatic (Wanamaker 1996). In most cases it is associated with the presence of a bone spur protruding in the nasal fossa, conflicting with the middle turbinate (less frequently with the inferior),

and therefore reducing the diameter of the middle meatus (Fig. 2.13).

Middle turbinate describing a lateral convexity toward the lateral sinusal wall is classified as paradoxical: this variant may hamper an endoscopic approach (Fig. 2.7f). When the bulbous segment is pneumatized, the middle turbinate is referred to as concha bullosa (Figs. 2.2, 2.8). If only the attachment portion of the middle turbinate is pneumatized – with no involvement of the bulbous segment – it is defined lamellar concha (Fig. 2.7f). According to the extent of pneumatization (vertical lamina, bulbous segment, or both) and its entity, this anomaly may narrow or obstruct the ethmoidal infundibulum as well as the middle meatus, and may interfere with nasal airflow, particularly if associated with other anomalies that may obstruct the OMU, such as a large ethmoidal bulla (Joe et al. 2000) (Fig. 2.13). The prevalence of middle turbinate pneumatization on CT studies varies from 14% to 53% (Lloyd 1990; Perez et al. 2000). Concha bullosa is often bilateral (Fig. 2.12) and associated with septal deviation.

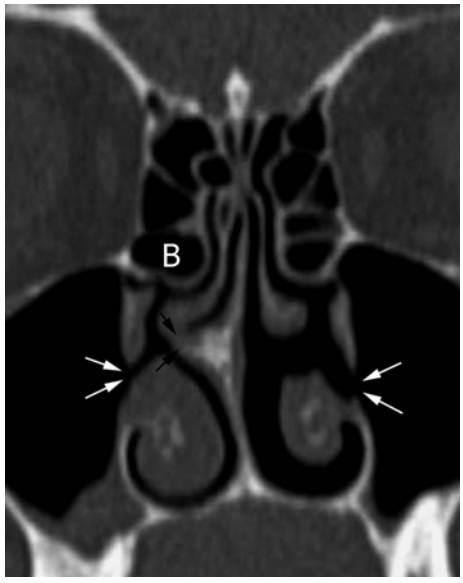

Fig. 2.13. Nasal septum deviation with a bone spur (*black arrows*) protruding into the right nasal fossa. An extensively pneumatized ethmoid bulla is present (*B*). Accessory maxillary sinus ostia (*white arrows*)

2.4.2 Uncinate Process

The most frequent variants are an anomalous curvature with the tip medially and downwardly oriented or the pneumatization of the uncinate process (up to 18% of subjects), the latter generally limited to the apex (uncinate bulla) (Bolger et al. 1991) (Figs. 2.2, 2.14). Seldom, a hypoplastic uncinate process, tightly

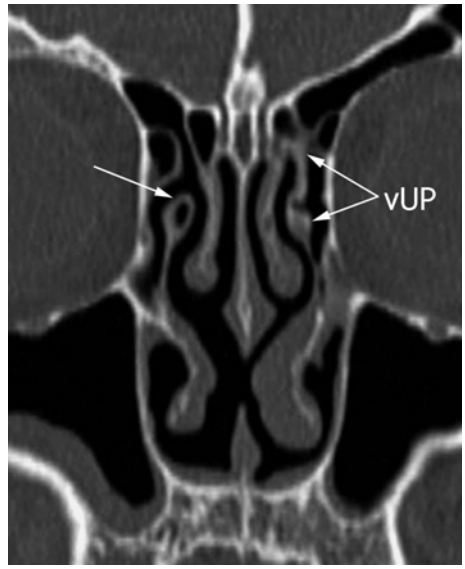

Fig. 2.14. Pneumatization of the vertical portion of the right uncinate process (*arrow*). The left inserts onto the fovea ethmoidalis [type 5 according to Landsberg and Friedman (2001)]. Note the focal nasal septum destruction due to cocaine abuse

adjacent to the lateral nasal wall or fused to the inferior aspect of the orbital floor or to the lamina papyracea, narrows the ethmoid infundibulum (*atelectatic infundibulum*). As a consequence underdevelopment of the maxillary sinus is observed along with intrasinusal mucous retention. In addition, the hypoplastic maxillary sinus is associated with a lower-than-normal location of the orbital floor. This variant has to be noted because of the higher risk of orbital damage at surgery. More rarely, the uncinate process may be absent.

2.4.3 Anterior Ethmoid Cells

During the development of ethmoid pneumatization, some cells may extend inferiorly and laterally to reach the medial orbital floor and the most inferior portion of the lamina papyracea, below the ethmoid bulla and lateral to the uncinate process *(infraorbital ethmoid cells or Haller cells*) (Fig. 2.15) (Stackpole and Edelstein 1997). When large in size, these cells may narrow the ethmoid infundibulum. Size and

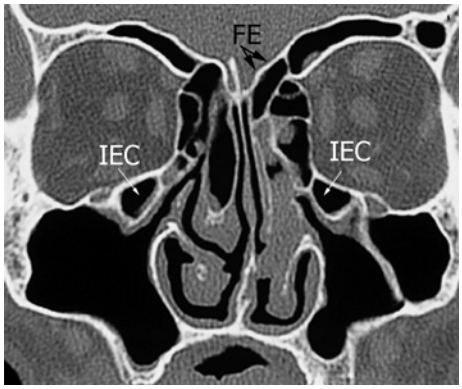

Fig. 2.15. Bilateral infraorbital ethmoid cells (*IEC*; Haller cells). *Black arrows* indicate the asymmetry of the fovea ethmoidalis (*FE*)

morphology of the ethmoid bulla are also highly variable: this cell may dislocate the ethmoid infundibulum and uncinate process (horizontalized). This variant has been considered by some authors to predispose for recurrent maxillary sinusitis. However, the definitive relationship between the presence of this variant and recurrent sinusitis is still debated (Stammberger and Wolf 1988; Bolger et al. 1991; Laine and Smoker 1992).

When extensively pneumatized, the ethmoid bullae may protrude into the middle meatus between the uncinate process and the middle turbinate and may narrow or obstruct the OMU (Figs. 2.3, 2.9, 2.13).

Agger nasi cells are the result of anterior extension of ethmoid cells to pneumatize the lacrimal bones (Figs. 2.6, 2.7, 2.9). Due to their location, agger nasi cells may obstruct the frontal recess.

Bulla frontalis indicates an ethmoid cell extending towards the frontal sinus. It is a rather complex variant and has been described in Sect. 2.1.3

2.4.4 Onodi Cells and Sphenoid Sinus

Onodi cells are the most hazardous variation since, if not reported before surgery, they may be a potential cause of severe complications. There are two definitions of Onodi cells in the literature. In the first they are defined as the most posterior ethmoid cells, superolateral to the sphenoid sinus and associated with a bulging, even if minimal, of the bony wall of the optic nerve (Kainz and Stammberger 1992) (Fig. 2.16). The second definition describes Onodi cells as posterior ethmoid cells extending into the sphenoid bone, either close to or impressed by the optic nerve bony wall (Stammberger and Kennedy 1995) (Fig. 2.17). The prevalence has been reported to range between 3.4% to 51%, this differ-

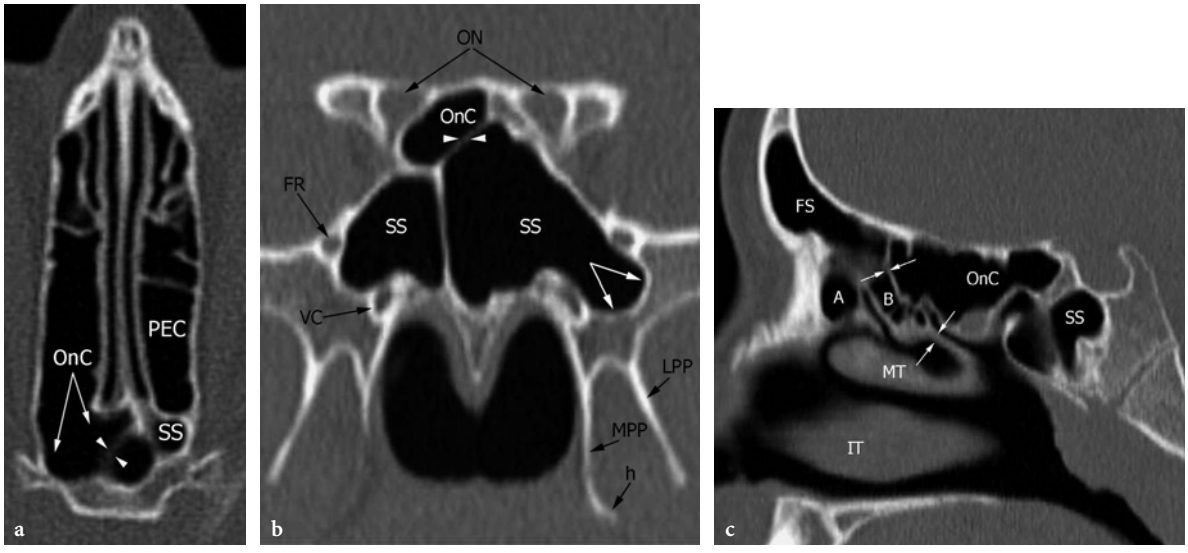

Fig. 2.16a–c. a On the axial plane the Onodi cell (*OnC*) arises on the right side from the posterior ethmoid and extends posteriorly and medially (*arrows*). **b** On the coronal plane the Onodi cell runs over the right and left sphenoid sinus roof (*arrowheads* indicate the thin left sphenoid sinus roof). The left sinus extends laterally into the pterygoid process (*arrows*). **c** On the sagittal plane a single large Onodi cell occupies the whole right posterior ethmoid sinus. *Opposite arrows* point to the ground lamella of the middle turbinate. Left posterior ethmoid cell (*PEC*), sphenoid sinus (*SS*), ethmoid bulla (*B*), frontal sinus (*FR*), agger nasi cell (*A*), middle (*MT*) and inferior (*IT*) turbinates, optic nerve and canals (*ON*), foramen rotundum (*FS*), vidian canal (*VC*), medial (*MPP*) and lateral (*LPP*) pterygoid plates, hamulus of medial pterygoid plate (*h*)

ence probably being related to the criteria used to classify this variant.

The sphenoid sinus itself displays highly variable degrees of pneumatization, including the anterior clinoid and pterygoid processes (Fig. 2.18). These variants may jeopardize endoscopic surgery, particularly when associated with focal areas of dehiscence of the bony walls of the sphenoid sinus. While a complete dehiscence of the bone covering the optic nerve (12%–22%) or the internal carotid artery (8%) has been infrequently found, a paper-thin bony lamina covering these bulgings has been observed more often (Kainz and Stammberger 1992; DeLano et al. 1996;).

It is important for the radiologist not only to detect thinning or dehiscences of the lateral sphenoid sinus walls but also to precisely assess the relationship of the sphenoid sinus and posterior ethmoid

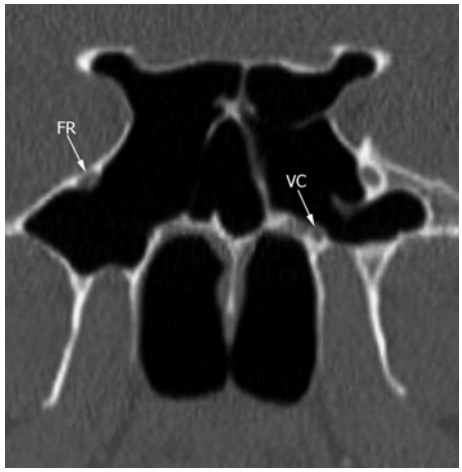

Fig. 2.18. Extensive pneumatization of the anterior clinoid and of the pterygoid processes of both sphenoid sinuses. Foramen rotundum (*FR*), vidian canal (*VC*)

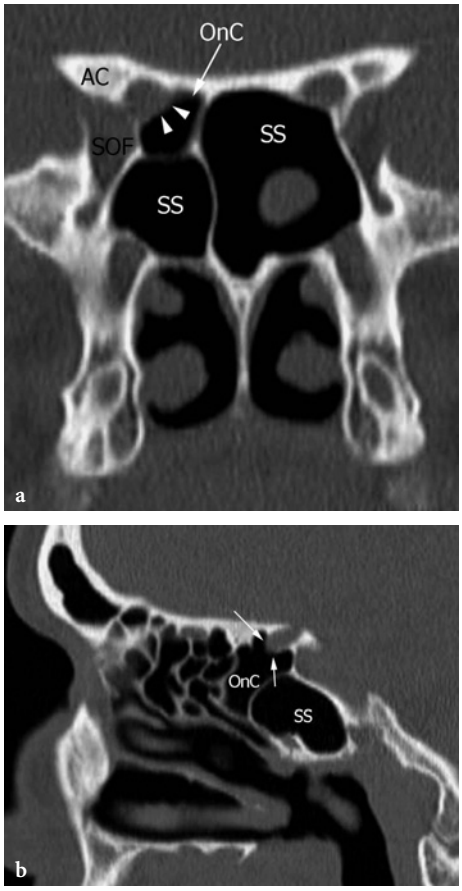

Fig. 2.17a,b. Right Onodi cell (*OnC*) associated with optic nerve canal dehiscence – *arrowheads* on (**a**), *arrows* on (**b**). Sphenoid sinus (*SS*), superior orbital fissure (*SOF*), anterior clinoid (*AC*)

cells with the internal carotid artery and the optic nerve. DeLano et al. (1996) classified the relationship with the optic nerve in four different types. In type 1, the nerve does not contact or impinge either the sphenoid or posterior ethmoid cells. In type 2, the nerve indents the sphenoid sinus, without contacting the posterior ethmoid cells. In type 3, the nerve runs through the sphenoid sinus, and it is surrounded by the pneumatized sinus for at least 50%. In type 4, the nerve courses close to both the sphenoid sinus and posterior ethmoid cells.

2.4.5 Asymmetry of Ethmoid Roof

The morphology of the ethmoid roof is usually inconstant. Asymmetry of the cribriform plate may be seen, directly related to the length of the vertical lamella, that inserts on it (Fig. 2.15). It has been observed in about 10% of patients (Dessi et al. 1994; Lebowitz et al. 2001). During surgery, this anomaly entails an increased risk of iatrogenic CSF fistulization or of injury of the anterior ethmoid artery, which courses along the most lateral aspect of the cribriform plate (Fig. 2.12). The depth of the ethmoid roof has been classified by Keros (1962) in three different types. In type 1 the vertical lamella of the cribriform plate is very short, therefore the olfactory fossa is almost flat; in type 2 the vertical lamella is longer, the olfactory fossa deeper; in type 3 the vertical lamella is particularly long (more than 13 mm) and the roof of the ethmoid is noticeably